

# UC Irvine

## UC Irvine Previously Published Works

### Title

Airborne measurement of inorganic ionic components of fine aerosol particles using the particle-into-liquid sampler coupled to ion chromatography technique during ACE-Asia and TRACE-P

### Permalink

<https://escholarship.org/uc/item/3f9440v0>

### Journal

Journal of Geophysical Research, 108(D23)

### ISSN

0148-0227

### Author

Lee, Y-N

### Publication Date

2003

### DOI

10.1029/2002jd003265

### Copyright Information

This work is made available under the terms of a Creative Commons Attribution License, available at <https://creativecommons.org/licenses/by/4.0/>

Peer reviewed

# Airborne measurement of inorganic ionic components of fine aerosol particles using the particle-into-liquid sampler coupled to ion chromatography technique during ACE-Asia and TRACE-P

Y.-N. Lee,<sup>1</sup> R. Weber,<sup>2</sup> Y. Ma,<sup>2</sup> D. Orsini,<sup>2</sup> K. Maxwell-Meier,<sup>2</sup> D. Blake,<sup>3</sup> S. Meinardi,<sup>3</sup> G. Sachse,<sup>4</sup> C. Harward,<sup>4</sup> T.-Y. Chen,<sup>5</sup> D. Thornton,<sup>6</sup> F.-H. Tu,<sup>6</sup> and A. Bandy<sup>6</sup>

Received 1 December 2002; revised 7 March 2003; accepted 28 March 2003; published 13 September 2003.

[1] Eight inorganic ions in fine aerosol particles ( $D_p < 1.3 \mu\text{m}$ ) were measured on board the NCAR C130 and NASA P-3B aircraft during the 2001 Aerosol Characterization Experiment (ACE)-Asia and the Transport and Chemical Evolution over the Pacific (TRACE-P) experiments, respectively. Concentrations of  $\text{NH}_4^+$ ,  $\text{SO}_4^{2-}$ ,  $\text{NO}_3^-$ ,  $\text{Ca}^{2+}$ ,  $\text{K}^+$ ,  $\text{Mg}^{2+}$ ,  $\text{Na}^+$ , and  $\text{Cl}^-$  were determined using a particle-into-liquid sampler coupled to ion chromatography (PILS-IC) technique at a 4-min resolution and a limit of detection  $< 0.05 \mu\text{g m}^{-3}$ . The maximum total ion concentrations observed on the C130 and the P-3B were  $27 \mu\text{g m}^{-3}$  and  $84 \mu\text{g m}^{-3}$ , respectively. During ACE-Asia,  $\text{NH}_4^+$  and  $\text{SO}_4^{2-}$  dominated, with the dust-derived  $\text{Ca}^{2+}$  contributing nearly equally as  $\text{SO}_4^{2-}$  in mixing ratios. The sea-salt-derived  $\text{Na}^+$  and  $\text{Cl}^-$  were comparable to biomass-burning tracer  $\text{K}^+$ , showing  $> 1$  ppbv only in the top 1% sample population. During TRACE-P,  $\text{NH}_4^+$  dominated, followed by  $\text{SO}_4^{2-}$ ,  $\text{Cl}^-$ ,  $\text{Na}^+$ ,  $\text{NO}_3^-$ ,  $\text{Ca}^{2+}$ , and  $\text{K}^+$ , in decreasing order of importance. In addition to a sea-salt origin,  $\text{Cl}^-$  showed a source in urban emissions possibly related to biofuel combustion. Both sea salt and dust contributed to  $\text{Mg}^{2+}$ . In both experiments,  $\text{NH}_4^+$ ,  $\text{SO}_4^{2-}$ ,  $\text{NO}_3^-$ , and CO were strongly correlated, indicating that combustion was the dominant source of these species and that  $\text{NH}_3$  and other alkaline materials were in sufficient supply to neutralize  $\text{H}_2\text{SO}_4$ . The  $[\text{NH}_4^+]$  to  $([\text{NO}_3^-] + 2[\text{SO}_4^{2-}])$  ratio was  $\sim 0.70$  in the two campaigns, with deviations found only in volcano plumes, whereby  $\text{SO}_4^{2-}$  was found to correlate with  $\text{SO}_2$ . Charge balance of the ions showed both positive and negative deviations whose magnitudes,  $\sim 30\%$ , provide estimates of the lower limits of unmeasured ions. Elevated  $\text{NO}_3^-$  and  $\text{Ca}^{2+}$  coexist mainly under polluted conditions, suggesting the importance of sequestering  $\text{HNO}_3$  by mineral dust. **INDEX**

**TERMS:** 0305 Atmospheric Composition and Structure: Aerosols and particles (0345, 4801); 0322 Atmospheric Composition and Structure: Constituent sources and sinks; 0365 Atmospheric Composition and Structure: Troposphere—composition and chemistry; 0368 Atmospheric Composition and Structure: Troposphere—constituent transport and chemistry; 0394 Atmospheric Composition and Structure: Instruments and techniques; **KEYWORDS:** Aerosol, Composition, PILS, TRACE-P, ACE-Asia

**Citation:** Lee, Y.-N., et al., Airborne measurement of inorganic ionic components of fine aerosol particles using the particle-into-liquid sampler coupled to ion chromatography technique during ACE-Asia and TRACE-P, *J. Geophys. Res.*, 108(D23), 8646, doi:10.1029/2002JD003265, 2003.

<sup>1</sup>Atmospheric Sciences Division, Brookhaven National Laboratory, Upton, New York, USA.

<sup>2</sup>School of Earth and Atmospheric Sciences, Georgia Institute of Technology, Atlanta, Georgia, USA.

<sup>3</sup>Department of Chemistry, University of California, Irvine, California, USA.

<sup>4</sup>NASA Langley Research Center, Hampton, Virginia, USA.

<sup>5</sup>Environmental Change Research Project, Academia Sinica, Taipei, Taiwan.

<sup>6</sup>Department of Chemistry, Drexel University, Philadelphia, Pennsylvania, USA.

## 1. Introduction

[2] Atmospheric aerosol particles play many important roles in the environment, including visibility, Earth radiation budget and human health effects [*National Research Council (NRC)*, 1998]. In order to establish models to predict the distribution of aerosol particles (in terms of size, number and chemical composition) and to assess their environmental and health effects, knowledge of the various types of aerosol sources from different regions of the world is needed. Since many Asian countries are experiencing increased energy consumption accompanying rapid economical growth, emissions related to man-made activities are expected to rise significantly. This increased emission can impact chemical composition of the atmosphere on a

regional to global scale and needs to be monitored to evaluate current effects and to predict future changes. In addition to emission sources related to man-made activities, natural sources of aerosol particles and their precursors also need to be understood. In Asia, both biomass burning and dust storms are important processes by which aerosol particles are generated.

[3] To gain an understanding of the emission sources in Asia, two large-scale field measurement programs were carried out in 2001 to record the chemical signals of outflows from eastern and southeastern Asia. Transport and Chemical Evolution over the Pacific (TRACE-P) was an aircraft-based campaign organized by the US National Aeronautics and Space Administration (NASA). This program deployed two large research aircraft, a DC-8 and a P-3B, to measure chemical composition off the coast of China, Taiwan, Japan and Korea during the period between 4 March and 4 April 2001. Aerosol Characterization Experiment (ACE)-Asia was organized by National Science Foundation (NSF) and National Oceanographic and Atmospheric Administration (NOAA) involving ground (in Taiwan, China and Korea), shipboard (NOAA R/V *Ron Brown*), and aircraft (NCAR C130) measurement platforms. The C130 flew mainly over the waters off the coast of China, Japan and Korea during the period between 30 March and 3 May 2001.

[4] Participating in both programs, we made real-time on-line measurement of the concentrations of inorganic ionic components in fine aerosol particles (i.e., aerodynamic size diameter  $<1.3\ \mu\text{m}$ ) on board the NASA P-3B and the NCAR C130 aircraft using the recently developed particle-into-liquid sampler coupled to ion chromatography (PILS-IC) technique [Weber *et al.*, 2001; Lee *et al.*, 2002; Orsini *et al.*, 2003].  $\text{NH}_4^+$ ,  $\text{SO}_4^{2-}$ ,  $\text{NO}_3^-$ ,  $\text{Ca}^{2+}$ ,  $\text{K}^+$ ,  $\text{Mg}^{2+}$ ,  $\text{Na}^+$ , and  $\text{Cl}^-$  were determined at a time resolution of 4 min and a limit of detection (LOD) of  $0.01 \sim 0.05\ \mu\text{g m}^{-3}$ . We present in this paper a brief description of the principles and operation of the PILS-IC instrument, and an overview of the data collected on the two aircraft regarding distributions, relationships, and possible sources of these chemical components. The simultaneously measured CO,  $\text{SO}_2$ , and several hydrocarbon species which provide insights as well as constraints are used to aid the characterizations. Additional analyses of the data regarding sources, transport/mixing, and chemical processing are to be reported elsewhere [e.g., Ma *et al.*, 2003].

## 2. Experimental Section

### 2.1. PILS-IC Instrument

[5] The PILS-IC instruments used on board the two aircraft were identical. A detailed description of the instrument in terms of construction, operation, efficiency, size selection, and calibrations is given elsewhere [Orsini *et al.*, 2003]. Briefly, the PILS-IC is consisted of four major components: gas denuders, a condensation particle growth chamber fitted with a steam generator, an impactor sample collector, and a dual-channel IC analysis system (Figure 1). Sample air drawn into the system ( $15.0\ \text{L min}^{-1}$ ) was first removed of potential gas interferents using two glass honeycomb denuders (Rupprecht & Patashnick Co., Inc. Albany, NY) placed in series immediately upstream of the

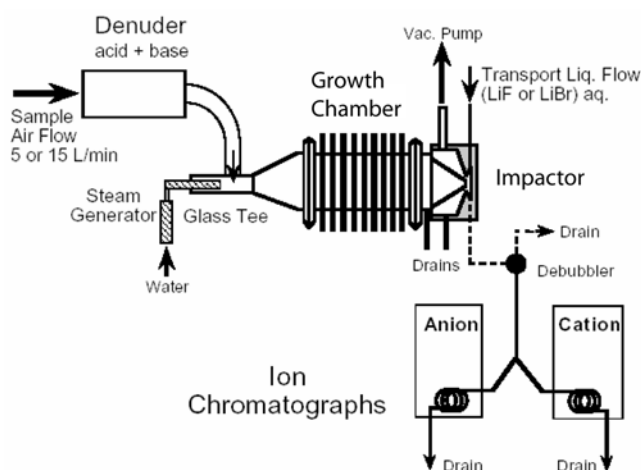


**Figure 1.** Schematic diagram of the PILS-IC instrument deployed on the NCAR C130 and NASA P-3B aircraft. Sample flow rate was  $15\ \text{L min}^{-1}$ .

condensation growth chamber. The two denuders were coated with  $\text{Na}_2\text{CO}_3$  and citric acid to remove acid gases (e.g.,  $\text{HNO}_3$  and  $\text{SO}_2$ ) and base gases (e.g.,  $\text{NH}_3$ ), respectively [Sioutas *et al.*, 1996], and were regenerated every other flight.

[6] The sample air entering into the condensation growth chamber was mixed with steam generated from heating a  $1.0\ \text{mL min}^{-1}$  liquid  $\text{H}_2\text{O}$  flow at  $110^\circ\text{C}$ , creating supersaturation conditions. Within the approximately 1 s residence time inside the chamber, particles were grown to supermicron sizes with an efficiency of  $\sim 90\%$  for particle diameters of 100 nm and greater [Orsini *et al.*, 2003]. The resulting supermicron size droplets were collected using an impactor designed with a  $D_{50} = 1\ \mu\text{m}$  [Marple and Willeke, 1976]. The small liquid sample collected on the impactor surface was washed off with a stream of  $\text{H}_2\text{O}$  (referred to as the carrier flow; flow rate =  $0.20\ \text{mL min}^{-1}$ ) and transported to the IC system for on-line analysis.

[7] The computer controlled IC system was comprised of one anion IC (Metrohm model 761 with a suppressor, equipped with a Metrohm Supp-5,  $4 \times 100\ \text{mm}$ , anion column) and one cation IC (Metrohm model 761 without a suppressor, equipped with a Metrohm Metrosep Cation 1-2,  $4 \times 125\ \text{mm}$ , column). The eluants were  $4.0\ \text{mM Na}_2\text{CO}_3/2.0\ \text{mM NaHCO}_3$  in  $\text{H}_2\text{O}$  for the anion IC, and  $4.0\ \text{mM}$  tartaric acid in  $10\% \text{CH}_3\text{CN}/\text{H}_2\text{O}$  for the cation IC. Both eluant flow rates were maintained at  $1.0\ \text{mL min}^{-1}$ . Since the actual sample volume (i.e., the collected droplets) varied depending on the concentration of condensable particles, the degree of dilution resulting from mixing the sample with the carrier flow also varied, albeit in a narrow range. To determine this dilution factor, a  $2.0\ \mu\text{M LiClO}_4$  was present in the carrier flow as an internal standard. The dilution factor was determined from the actual concentration of  $\text{Li}^+$  measured by the IC.

### 2.2. Inlet Systems and Particle Size Selection

[8] The aerosol inlets on the C130 and the P-3B were different: the C130 featured a Low Turbulence Inlet (LTI) which allowed high transmission efficiencies for supermicron size aerosol particles and the P-3B used a shrouded

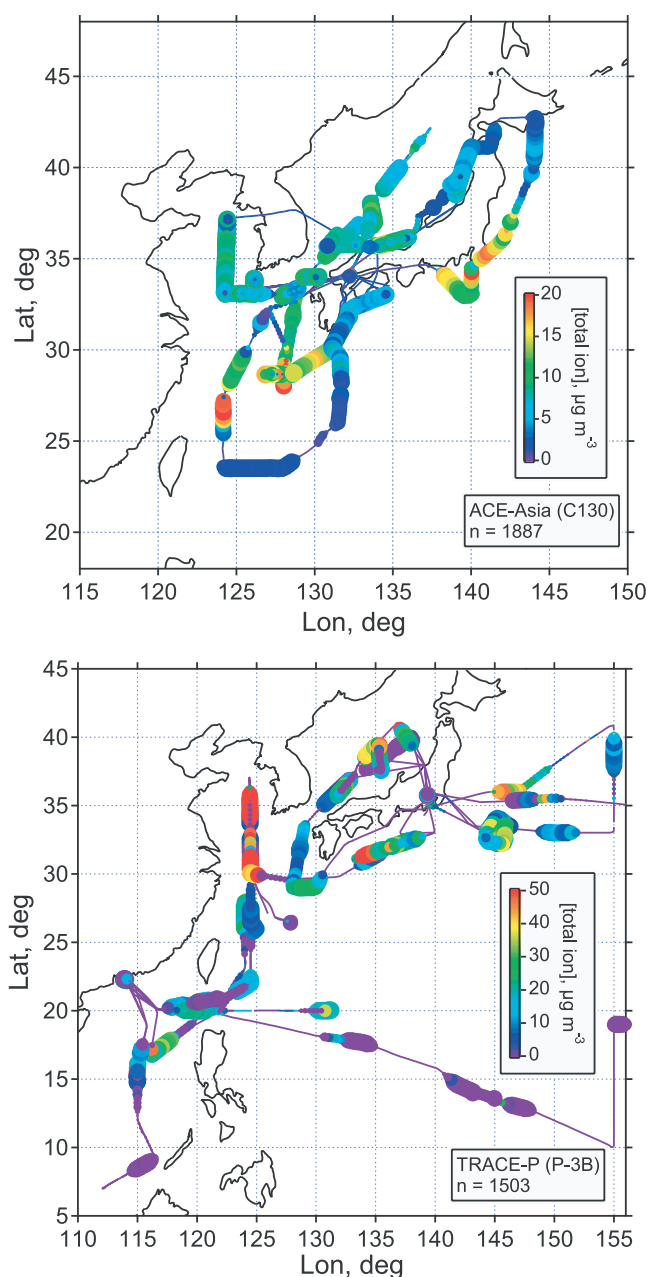


**Figure 2.** Flight tracks of the NCAR C130 and NASA P3-B during ACE-Asia and TRACE-P, respectively. The total measured ion concentrations are color-coded according to the color bars (the maximum concentrations are beyond that indicated by the color bars); large symbols denote altitudes below 3 km, narrow lines denote altitudes above 3 km, and intermediate symbols denote altitudes between 2.7 and 3 km. The total numbers of PILS-IC samples are indicated.

inlet which maintained a constant turbulence characteristics in the diffuser cone independent of the attack-angle. Because the PILS system on the P-3B was situated across the aisle from the inlet, there was an additional  $\sim 8$  ft of tubing length (conductive, id = 0.75 in) between the inlet and the instrument compared to the C130 configuration. However, in spite of these differences, calculations showed that aerosol transmission efficiencies for size range 80 nm to 2.5  $\mu\text{m}$  were greater than 99% in both systems.

[9] A more restrictive size-cut limitation was identified during post-experiment characterizations of the PILS system. This restriction was caused by a bend in the sample air-steam mixing region of the PILS used in the experiments and was found to effect a size cut of  $\sim 1.3 \mu\text{m}$  at the 15.0 L  $\text{min}^{-1}$  sample flow rate used [Orsini *et al.*, 2003]. As a result, the term fine aerosols used in our work has an upper size cut of 1.3  $\mu\text{m}$ . Further, it was found out that the instrument's sampling efficiency for smaller particles leveled off at  $\sim 90\%$  [Orsini *et al.*, 2003], agreeing with the filter data also collected on the P-3B for calibration purpose. The final data have been corrected for this efficiency factor.

### 2.3. Other Measurements

[10] Hydrocarbons were determined by taking whole air samples in electro-polished canisters followed by laboratory GC-FID-MS analysis [Blake *et al.*, 1997]. CO was measured by a tunable diode laser absorption spectroscopy technique [Sachse *et al.*, 1991] and  $\text{SO}_2$  by a chemical ionization mass spectrometry technique [Thornton *et al.*, 2002].

### 2.4. Flight Summary

[11] A total of 19 research flights were performed on each aircraft. All of the 19 flights of the NCAR C130, which was stationed in Iwakuni, Japan, were made over Japan, South Korea, the Yellow Sea, East China Sea, and the Sea of Japan (between latitude  $23^\circ$ – $43^\circ\text{N}$  and longitude  $124^\circ$ – $144^\circ\text{E}$ , Figure 2). In contrast, the NASA P-3B devoted 7 of its flights over the Pacific Ocean during the transits between California and Asia, leaving 12 flights covering the western Pacific region including South China Sea and the regions mentioned above. We limit our analysis of the P-3B data to those collected in this region, i.e., latitude  $7^\circ$ – $41^\circ\text{N}$  and longitude  $112^\circ$ – $156^\circ\text{E}$  (Figure 2). During this western Pacific research phase, the P-3B was stationed in Hong Kong, Okinawa, and Yokota, Japan. The two aircraft missions overlapped for a 5 day period during which two intercomparison flights were conducted, one on 30 March 2001 and the other 1 April 2001. Concerning the PILS measurement, no data were obtained on the C130 on the 1 April 2001 flight because of a logistic problem. Intercomparison of the PILS-IC data collected on the two aircraft on 30 March 2001 is reported by Y. Ma *et al.* (manuscript in preparation, 2003). The ceilings of the two aircraft were comparable: 7 km and 8 km for the P-3B and the C130, respectively. The flight durations were 8–10 hr.

## 3. Results and Discussion

[12] PILS-IC data were collected on all of the 19 flights on the P-3B. For the C130 the data were missing on 3 flights: RF02 (1 April 2001), RF03 (4 April 2001) and RF19 (3 May 2001). The total ion concentrations (the sum of the measured ions) are coded in color and displayed along the flight tracks (Figure 2) to show the locations where elevated fine aerosol mass loadings were encountered. The vertical distributions of the ions and the total ion mass concentration in three latitude bands are shown in Figures 3 and 4, respectively. The solid lines in Figure 4 represent the locally weighted regression scatterplot smoothing (Lowess) fits which closely track the median values. We used the Lowess fit because it is more



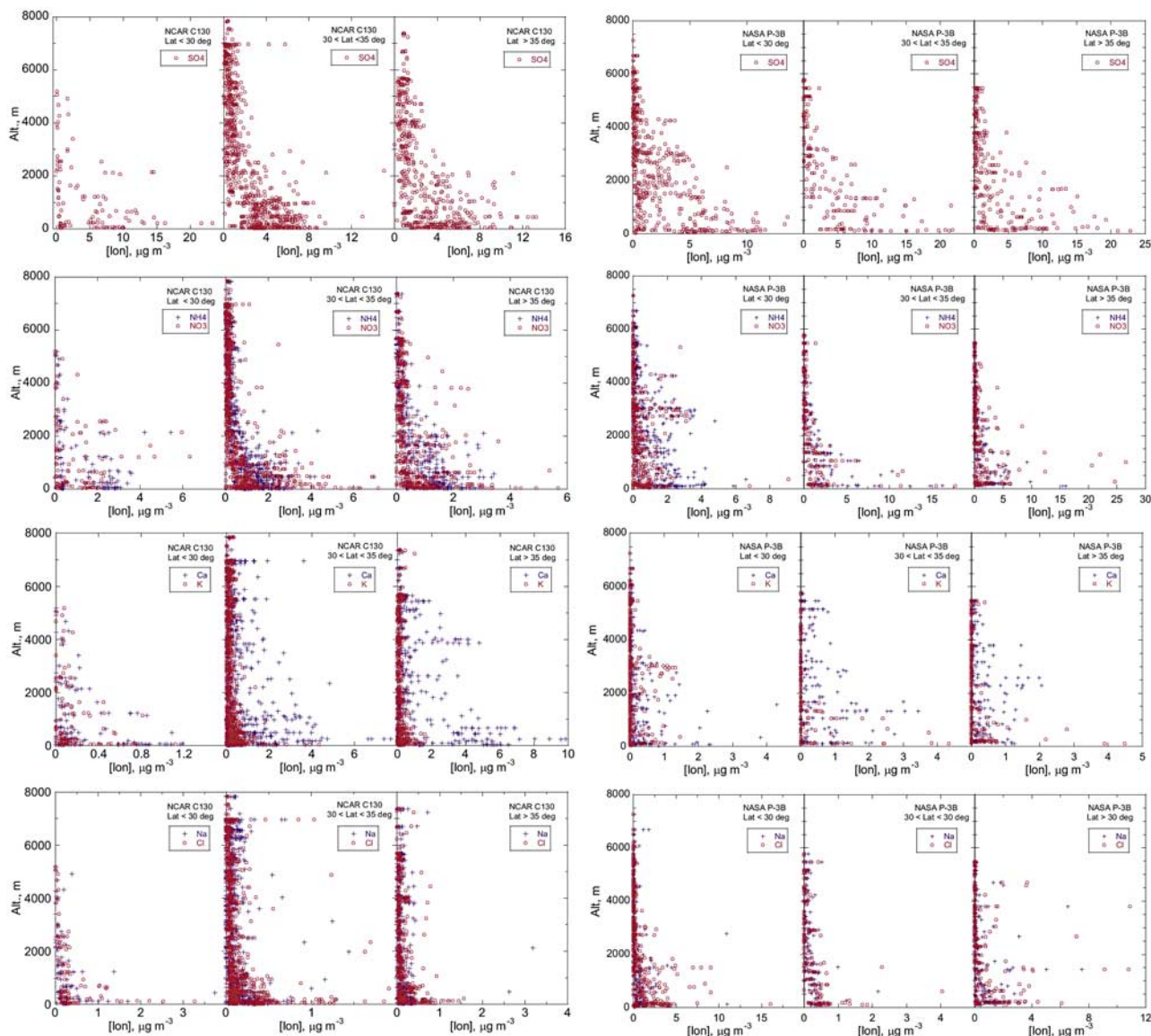


**Figure 3.** Vertical distributions of  $\text{SO}_4^{2-}$ ;  $\text{NH}_4^+$ ,  $\text{NO}_3^-$ ;  $\text{Ca}^{2+}$ ,  $\text{K}^+$ ; and  $\text{Na}^+$ ,  $\text{Cl}^-$  in three latitude bands ( $^{\circ}\text{N}$ ):  $<30$ ,  $30 < \text{latitude} < 35$ , and  $>35$ .

convenient than the common practice of showing box plots of binned data.

[13] Because  $\text{NH}_4^+$ ,  $\text{NO}_3^-$ , and  $\text{SO}_4^{2-}$  all showed much lower concentrations above 3 km (Figure 3), we used this altitude as an approximate division between the mixed layer and the free troposphere for displaying the probability plots of the ions (Figure 5). The maximum total ion concentration observed on the P-3B ( $84 \mu\text{g m}^{-3}$ ) was significantly higher than that of the C130 ( $27 \mu\text{g m}^{-3}$ ) mainly because of the encounter of a highly polluted air mass over the Yellow Sea (flight 14, 18 March 2001, Figure 6). Concentrations of  $\text{Na}^+$  and  $\text{Cl}^-$  were both higher on the P-3B, but  $\text{K}^+$  concentrations were roughly comparable. The C130 however intercepted air masses that contained much higher fine soluble  $\text{Ca}^{2+}$  than the P-3B (Figure 5), the maximum being 9.9 versus  $4.3 \mu\text{g m}^{-3}$ .

### 3.1. Relationships Between the Ions

[14] The individual chemical species are useful tracers for identifying their sources [e.g., *Andreae and Merlet, 2001*].

The relationship between these species, with or without a correlation, provides additional support for such analyses.  $\text{Na}^+$  and  $\text{Cl}^-$  are thought to be primarily derived from sea-salt aerosols especially in marine environment where the ACE-Asia and TRACE-P experiments were conducted. During ACE-Asia the plot of  $\text{Cl}^-$  against  $\text{Na}^+$  showed a slope of 1.04 with  $r^2 = 0.85$  (Figure 7), fairly close to the seawater ratio of 1.16. Several data points showing high  $\text{Na}^+$  but very low  $\text{Cl}^-$  were not used in the regression. Whether these data points are real or caused by measurement uncertainties is unknown and is being investigated. The slightly lower than seawater ratio observed is consistent with acidification of particles by strong acids  $\text{H}_2\text{SO}_4$  and  $\text{HNO}_3$ , resulting in a  $\text{Cl}^-$  deficit through  $\text{HCl}$  volatilization. The correlation between  $\text{Cl}^-$  and  $\text{Na}^+$  observed on the P-3B showed a higher slope of 1.4 (Figure 7), suggesting possible additional sources of  $\text{Cl}^-$  other than sea-salt aerosols. Since the three highest  $\text{Cl}^-$  points were found at altitude of 3–4 km and were associated with moderate  $\text{Ca}^{2+}$  concen-

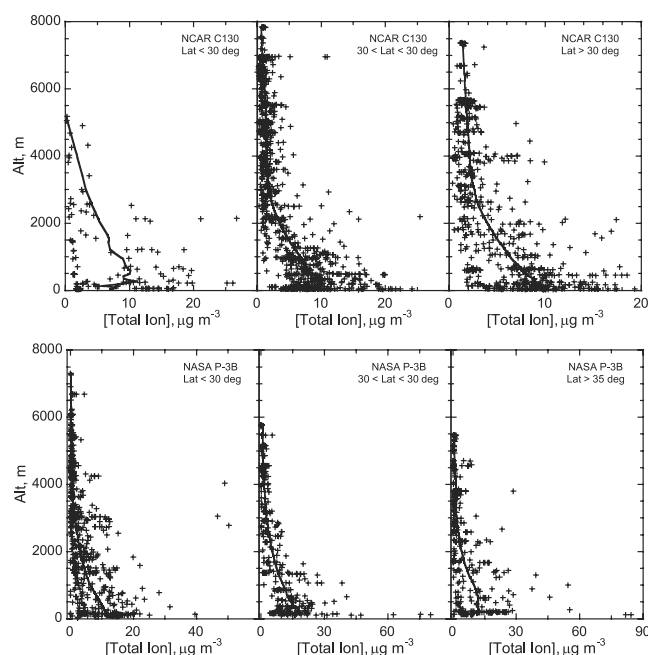


**Figure 4.** Vertical distributions of the total ion mass concentrations segregated by latitude. The solid lines represent locally weighted average.

trations,  $\sim 500$  pptv, a source of  $\text{Cl}^-$  in crustal material cannot be ruled out. In addition, we also note that  $\text{Cl}^-$  and  $\text{Na}^+$  observed in the polluted air mass during NASA P-3B flight 14 (Figure 6) showed a higher ratio than those observed in cleaner air masses. While the points below the seawater ratio line (Figure 8) may be caused by the  $\text{Cl}^-$  loss mechanism mentioned above, the points above the seawater ratio line indicate that there are additional sources of  $\text{Cl}^-$  that are associated with urban pollution which can significantly influence the  $\text{Cl}^-/\text{Na}^+$  ratio. This observation is consistent with the report by *Ye et al.* [2003] that while the mean  $\text{Na}^+$  concentrations in Shanghai City were nearly constant over the 4 seasons ( $0.41\text{--}0.62\ \mu\text{g m}^{-3}$ ), mean  $\text{Cl}^-$  concentrations increased significantly from summer ( $0.22\ \mu\text{g m}^{-3}$ ) to winter ( $3.54\ \mu\text{g m}^{-3}$ ). The fact that the samples showing elevated  $\text{Cl}^-$  also contained high levels of  $\text{K}^+$  (Figure 8), a biomass-burning tracer [*Ma et al.*, 2003], strongly suggests that the urban source of  $\text{Cl}^-$  is related to combustion of biofuel. This argument is consistent with the findings of *Ye et al.* [2003] that  $\text{K}^+$  was also elevated in Shanghai during the winter season.

[15]  $\text{Ca}^{2+}$  is generally believed to be derived from soil and crustal material, and can therefore be used as a tracer for wind blown dusts from deserts and arid regions [e.g., *Wang et al.*, 2002]. The major forms in which calcium is found as crustal material, e.g., calcite/dolomite, are sufficiently soluble and form  $\text{Ca}^{2+}$  through hydrolysis and/or reaction with acids. Minor forms of calcium such as  $\text{Ca}_3(\text{PO}_4)_2$  may not contribute to the measured  $\text{Ca}^{2+}$  because of their limited solubilities. In addition to this commonly accepted association between aerosol  $\text{Ca}^{2+}$  and its dust/crustal material origin, we are also considering the possibility that construction activities (and cement manufacturing) in major urban areas may also play a role in aerosol  $\text{Ca}^{2+}$  content. We note that elevated  $\text{Ca}^{2+}$

concentrations were detected in the most polluted plume encountered in the TRACE-P mission (P-3B flight 14, Figure 6), which has a strong urban emission characteristics judging from the high concentrations of aerosol nitrate, sulfate and many hydrocarbon species. The observed  $\text{K}^+$  to  $\text{Ca}^{2+}$  ratio of  $\sim 3$  in the first encounter of this plume (Figure 6) is similar to the ratios of the mean concentrations of these species reported for Shanghai City ( $\sim 4$  in winter [*Ye et al.*, 2003]), suggesting that an urban source of  $\text{Ca}^{2+}$  may be important and needs to be further characterized.

[16] In the C130 data set,  $\text{Mg}^{2+}$  showed a correlation with  $\text{Ca}^{2+}$  ( $r^2 = 0.83$ ) with a slope of 0.12, but not with  $\text{Na}^+$  despite the fact that some high  $\text{Mg}^{2+}$  points are associated with elevated  $\text{Na}^+$  (Figure 9). However, in the P-3B data set, we note that  $\text{Mg}^{2+}$  at elevated concentrations ( $>400$  pptv) were correlated with  $\text{Na}^+$  ( $r^2 = 0.78$ ) exhibiting a  $\text{Mg}^{2+}$  to  $\text{Na}^+$  ratio of 0.08. This slope is fairly close to their seawater ratio of 0.11. When these high  $\text{Mg}^{2+}$  points are removed, a lower  $\text{Mg}^{2+}$  to  $\text{Ca}^{2+}$  ratio of 0.16 resulted ( $r^2 = 0.69$ ), similar to that found on the C130. That sea-salt particles are found to contribute to  $\text{Mg}^{2+}$  observed on the P-3B is consistent with the general conditions the two aircraft platforms had experienced: the C130 had seen more dust than sea salt and the P-3B the opposite.

[17]  $\text{K}^+$  showed a moderate correlation with  $\text{NH}_4^+$  and  $\text{NO}_3^-$ ,  $r^2$  being 0.47 and 0.64, respectively, during ACE-Asia, and 0.58 and 0.55 during TRACE-P. Because  $\text{K}^+$  is thought to be associated with biomass burning (including biofuel [*Ma et al.*, 2003]), these correlations suggest that both  $\text{NH}_4^+$  and  $\text{NO}_3^-$  have an appreciable source in these processes. It may be pointed out that the fact that elevated  $\text{K}^+$  concentrations were observed in a highly polluted urban plume (Figure 6) strongly supports that biofuel is an important source of this aerosol component. *Ye et al.* [2003] showed that  $\text{K}^+$  was important in the Shanghai urban areas and that the mean concentration increased by  $\sim 3$  fold from summer ( $0.89\ \mu\text{g m}^{-3}$ ) to winter ( $3.2\ \mu\text{g m}^{-3}$ ), corroborating the elevated  $\text{K}^+$  we measured.

[18]  $\text{NH}_4^+$  was strongly correlated with  $\text{NO}_3^-$  and  $\text{SO}_4^{2-}$  ( $r^2$  being 0.66 and 0.69, respectively, during both ACE-Asia and TRACE-P), and stronger still with the sum of  $\text{NO}_3^-$  and  $\text{SO}_4^{2-}$  (Figure 10), suggesting that  $\text{NH}_3$  shared common emission sources with  $\text{NO}_3^-$  and  $\text{SO}_4^{2-}$  and their precursors. One may note that  $\text{NH}_3$  is emitted at a significant level ( $\sim 1\%$  of CO) from vehicles equipped with the modern 3-way catalytic converters [*Perrino et al.*, 2002]. If a slope of unity was observed in these plots (Figure 10), then a complete neutralization by  $\text{NH}_3$  of  $\text{HNO}_3$  and  $\text{H}_2\text{SO}_4$  is indicated. However, since the best fit slope was 0.68, it indicates that on average there is a  $\sim 30\%$  of deficit in  $\text{NH}_4^+$  compared to  $\text{NO}_3^-$  and  $\text{SO}_4^{2-}$ . This deficit is therefore made up by other cations, including unmeasured organic species (e.g., amines), soil-derived species (e.g., Fe and Mn) and the hydronium ion (acid aerosols). However, since  $\text{H}_2\text{SO}_4$  is a much stronger acid than  $\text{HNO}_3$  and exhibits a negligible vapor pressure compared to  $\text{HNO}_3$ , aerosol  $\text{NO}_3^-$  resulting from condensation of gas phase  $\text{HNO}_3$  with available  $\text{NH}_3$  (or other alkaline reagents) will become important only if  $\text{H}_2\text{SO}_4$  is fully neutralized [*Seinfeld and Pandis*, 1997]. Consequently, the presence of  $\text{NO}_3^-$  in aerosols can be used to indicate that the aerosol particles are no longer acidic, and to assess the relative source strengths of

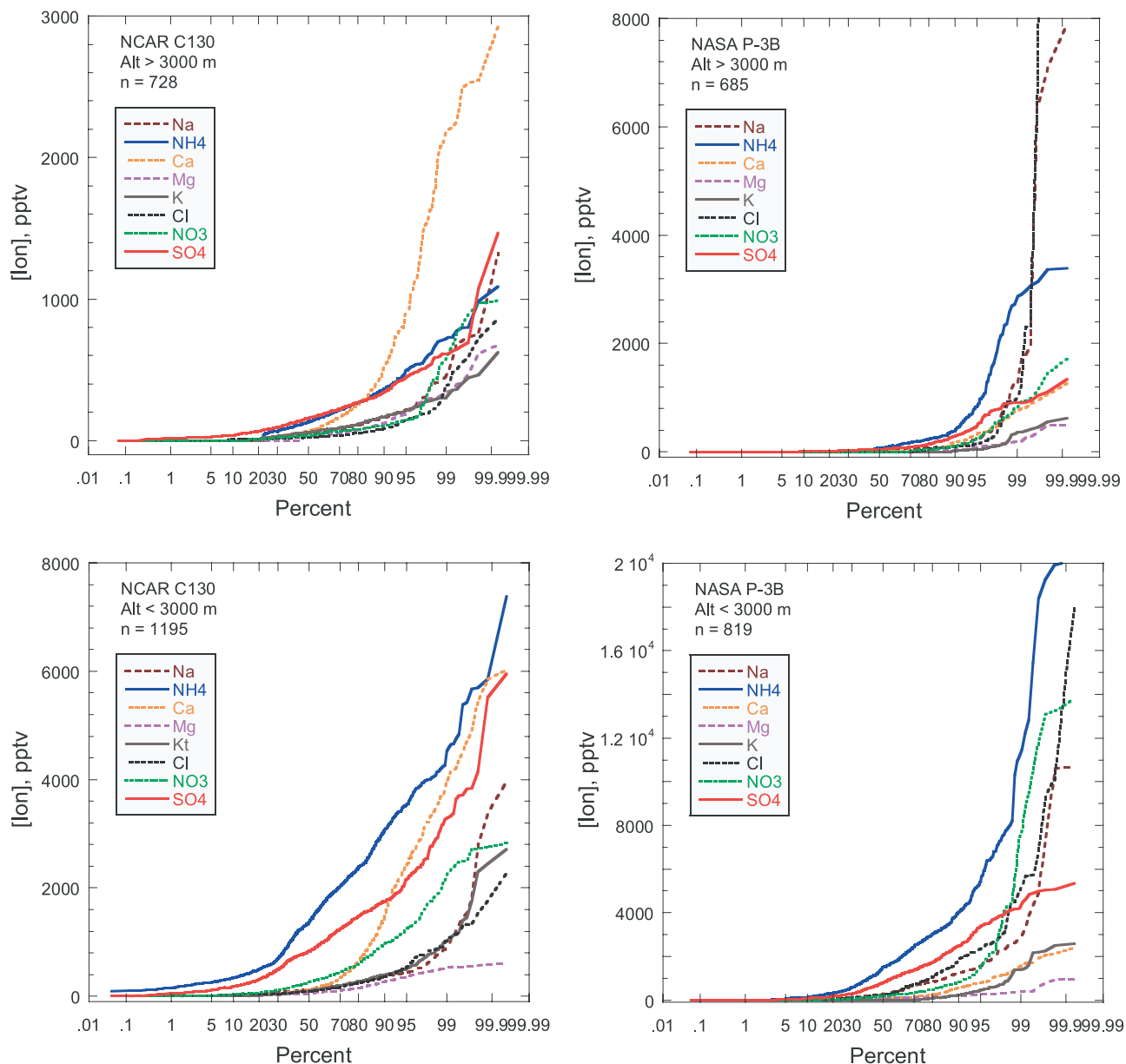


**Figure 5.** Frequency distributions of fine aerosol ionic components in two different altitude ranges: below and above 3 km.

$\text{NH}_3$  and the total sulfur (dominated by  $\text{SO}_2$  near emission sources). From the fact that >90% of the samples collected below 3 km, i.e., 1133 out of the 1161 collected on the C130 and 729 out of the 812 on the P-3B, contained nonzero  $\text{NO}_3^-$  (i.e.,  $[\text{NO}_3^-]/[\text{SO}_4^{2-}] > 0.02$ ), we conclude that under most conditions  $\text{NH}_3$  and other alkaline materials, e.g., amines, were emitted in quantities comparable to or greater than  $\text{H}_2\text{SO}_4$  and its precursor  $\text{SO}_2$ .

[19] The altitude dependence of the ratio of  $\text{NH}_4^+$  to the sum of  $\text{NO}_3^-$  and  $\text{SO}_4^{2-}$  is shown in Figure 11. The Lowess fits shown as the solid lines, which approximates the median, indicate for the C130 data a slight negative departure from the best fit slope of 0.68 in the 3 to 6 km range and a positive departure above 6 km. For the P-3B data, the ratio decreased from  $\sim 0.8$  at lower altitudes to  $\sim 0.5$  at higher altitudes. In both experiments, this ratio remained fairly constant below 3 km and showed departures only

above this altitude. This behavior qualitatively agrees with the 3 km height chosen to divide the mixed layer and the free troposphere (Figure 5) for which air masses of different sources and history are likely to be encountered.

[20] The co-emission of  $\text{NH}_3$  along with aerosol sulfate and its precursor  $\text{SO}_2$  is also observed during a study of the plumes of the Miyakejima volcano (24.08N, 139.53E, P-3B flight 17, 27 March 2001). Sampling was carried out downwind of the volcano approximately 200 to 300 km to the east southeast. The molar ratio of  $[\text{NH}_4^+]$  to  $2[\text{SO}_4^{2-}]$  decreased with increasing aerosol  $\text{SO}_4^{2-}$ , reaching an asymptotic value of  $0.42 \pm 0.016$  (Figure 12). Because the analysis was confined to samples associated with the volcano plumes (altitude < 2 km;  $[\text{SO}_2] > 2$  ppbv), the reaching of an  $\text{NH}_4^+$  to  $\text{SO}_4^{2-}$  equivalent ratio at 0.42 indicates that  $\text{NH}_3$  was released at a molar ratio roughly similar to that of  $\text{SO}_2$ . Because we expect a titration behavior

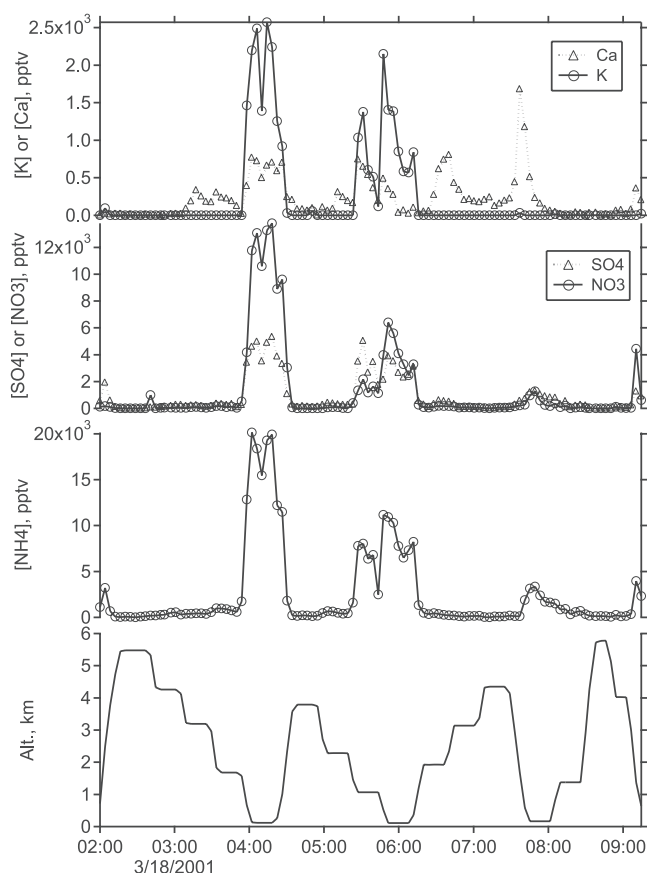


**Figure 6.** Time series of the concentrations of several fine aerosol ionic components observed during NASA P-3B flight 14 (18 March 2001) where a most polluted air mass during the entire mission was encountered.

in the  $[\text{NH}_4^+]/[\text{SO}_4^{2-}]$  ratio if  $\text{NH}_3$  is the only neutralizing reagent, the fact that the ratio reached an asymptotic value of 0.42 without showing an end point strongly suggests the presence of other alkaline materials. We speculate that amines and alkaline metals were among the candidates. It is noted that  $\text{SO}_4^{2-}$  was correlated with  $\text{SO}_2$  (Figure 13) suggesting that the oxidation of  $\text{SO}_2$  to  $\text{H}_2\text{SO}_4$  is the rate limiting step of aerosol  $\text{SO}_4^{2-}$  production.

### 3.2. Charge Balance

[21] Electrical charge balance of the observed aerosol ionic components offers insights into whether the major ionic species comprising the aerosol particles have been identified and quantified. Further, in the case of departure from neutrality, we may estimate the possible identities of the missing ionic species and their contributions. In addition, measurement reliability can also be evaluated through this inspection.

[22] In Figure 14 we plot the total positive charges against the total negative charges (in pptv-equivalent) found in the samples. For the C130, the best fit shows a slope of 0.91 and a large intercept of 648 pptv-equivalent. The correlation coefficient of this scatterplot is 0.67, reflecting the fairly sizable scatter of the data. However, we note that all the points lie above the 1:1 ratio line contained elevated levels of  $\text{Ca}^{2+}$ , i.e.,  $[\text{Ca}^{2+}] > 1.0 \mu\text{g m}^{-3}$ . A plausible explanation

of this observation is that the anions associated with  $\text{Ca}^{2+}$  were not completely identified by our measurement technique. A possible candidate of this missing anion is  $\text{CO}_3^{2-}$ , which is known to be associated with crustal material derived  $\text{Ca}^{2+}$  and was not quantified by our IC technique.

[23] To examine whether all of the anions associated with  $\text{Ca}^{2+}$  were undetected and therefore resulted in the large positive deviations seen in Figure 14, we inspect the same plot but with  $\text{Ca}^{2+}$  removed. While the correlation coefficient increased to 0.80, the best fit slope only slightly lowered to 0.82, with large scatters evenly distributed about the 1:1 line. This indicates that the  $\text{Ca}^{2+}$  rich samples with potentially unquantified anions contributed only a portion of

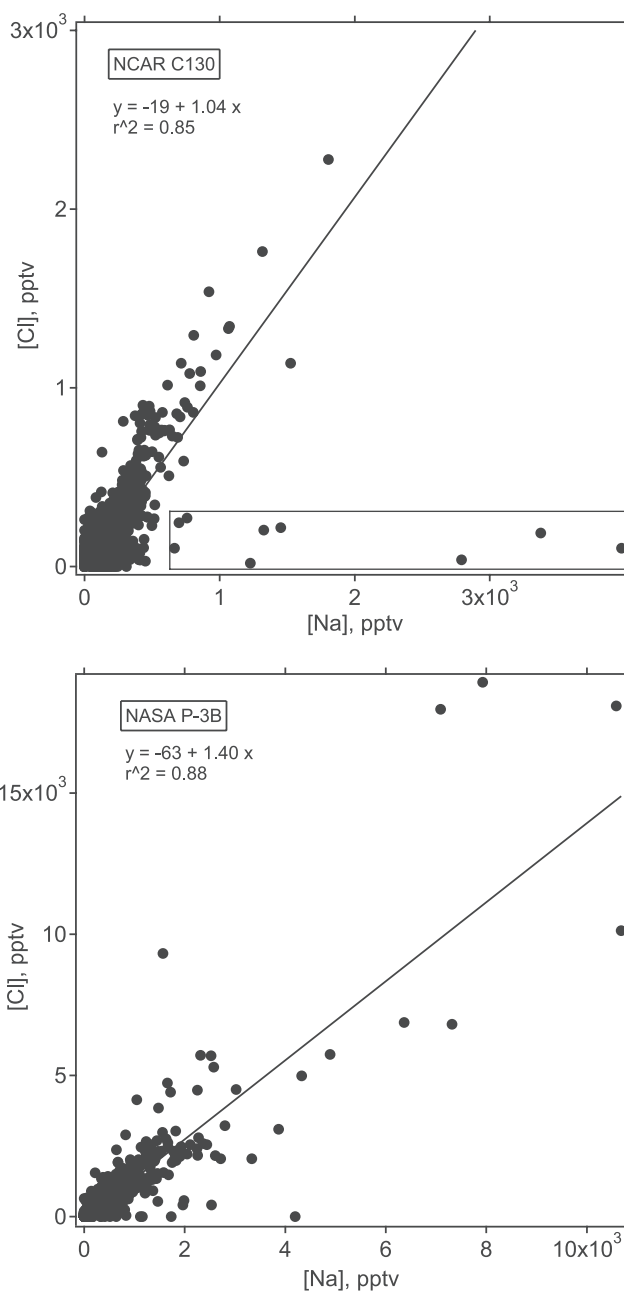


**Figure 7.** Correlation between aerosol  $\text{Cl}^-$  and  $\text{Na}^+$ . The solid lines represent the least squares fits. Data points in the rectangular box were not used in the regression.



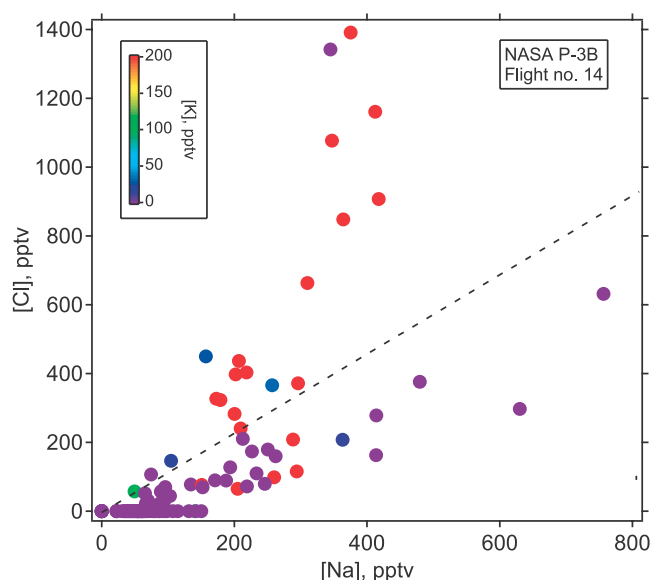


**Figure 8.** Scatterplot of  $\text{Cl}^-$  versus  $\text{Na}^+$  observed on NASA P-3B flight 14. The dashed line represents their seawater ratio of 1.16. Data points are color-coded according to  $\text{K}^+$  concentration which extends beyond the indicated range.

the positive deviation in the charge balance. It was noted that neither  $\text{Cl}^-$  nor  $\text{SO}_2$  caused a bias in the observed scatter; data points with high values of these two species being evenly distributed about the 1:1 ratio line. With the aerosol chemical composition knowledge established so far [e.g., Seinfeld and Pandis, 1997], we recognize that organic compounds are also important components of aerosols and may contribute to the missing charges. Excess negative charges reflect the presence of unmeasured cations, including metals, amines and strong acids. Excess positive charges, on the other hand, indicate unmeasured anions such as carboxylates [Kawamura and Sakaguchi, 1999]. The data points (Figure 14) exhibiting the largest negative deviations, i.e., those identified in Figure 10 (small size circles) having the lowest ratio of  $\text{NH}_4^+$  to  $(\text{NO}_3^- + \text{SO}_4^{2-})$ , may contain the strong acid,  $\text{H}_2\text{SO}_4$ , that has not been fully neutralized. However, because  $\text{NO}_3^-$  was present in most of the samples as pointed out earlier, acid aerosols can only account for an upper limit of 10% of the samples.

[24] The plots of total positive to negative charges are shown in Figure 15 for the P-3B data. As with the C130 data, samples containing higher  $\text{Ca}^{2+}$  tend to lie above the 1:1 line. The best fit slope, 0.83, is similar to that of the C130 data with  $\text{Ca}^{2+}$  removed. However, we note that samples corresponding to high  $\text{SO}_2$  concentrations were responsible for a low positive to negative charge ratio. The red points in Figure 15 (bottom panel) with  $\text{SO}_2$  in excess of 10 ppbv were identified to be those collected in the Miyakejima volcano plumes during P-3B flight 17. It is also interesting to point out that most of the high  $\text{SO}_2$  points not associated with the volcano plumes showed a charge balance very close to unity, again supporting the notion that alkaline materials, principally  $\text{NH}_3$ , is co-emitted at a level similar to or possibly greater than the acid aerosols and their precursors. There are

fewer data points in Figure 15 (bottom panel) because  $\text{SO}_2$  was not determined on all of the P-3B flights.

[25] The magnitude of the charge imbalance, i.e., total positive charges minus total negative charges, is plotted in Figure 16 as a function of the total concentration of the ions. With respect to the C130 data, the Lowess fit of the negative deviations showed a “median” of  $-60\%$  at the lowest total ion concentration which then decreased to  $-18\%$  at 3 ppbv and remained at that level for the higher concentration regime. The Lowess fit of the positive deviations reduced from 50% at the lowest concentrations to 40% at 3 ppbv, and then remained between 30 to 35% in the higher concentration range. The P-3B data showed a similar

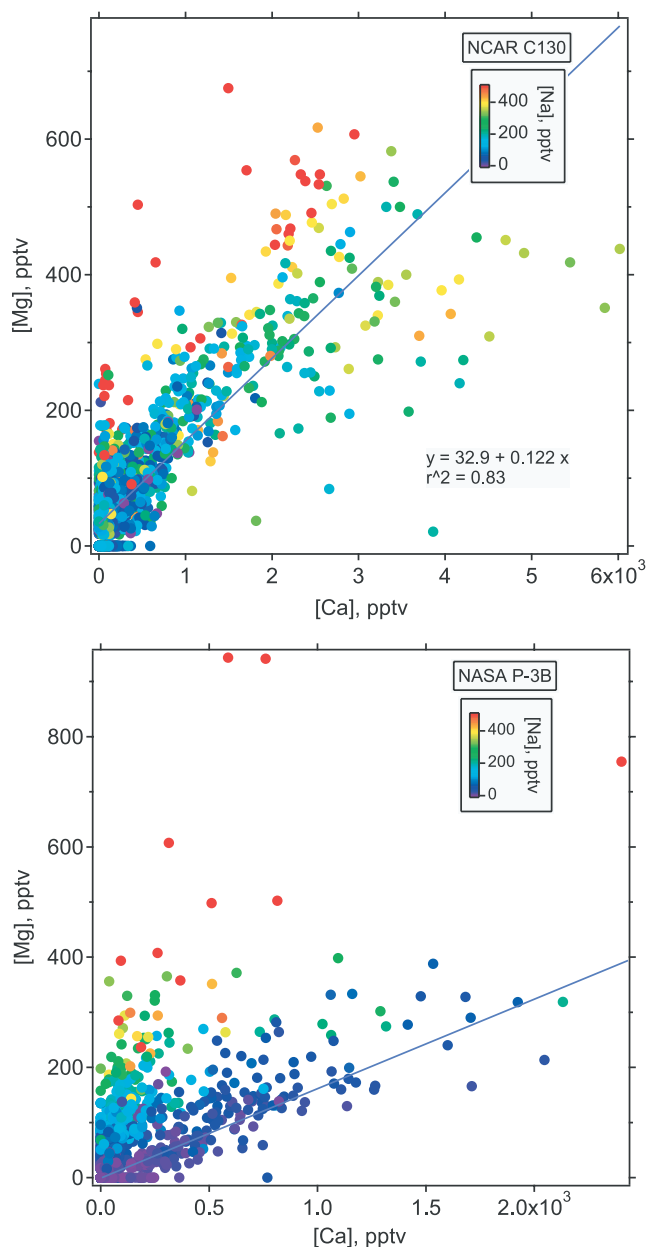


**Figure 9.** Correlation between  $\text{Mg}^{2+}$  and  $\text{Ca}^{2+}$  with the data points color-coded to  $\text{Na}^+$  concentration. The solid lines in both panels represent the best fit of the NCAR C130 data.

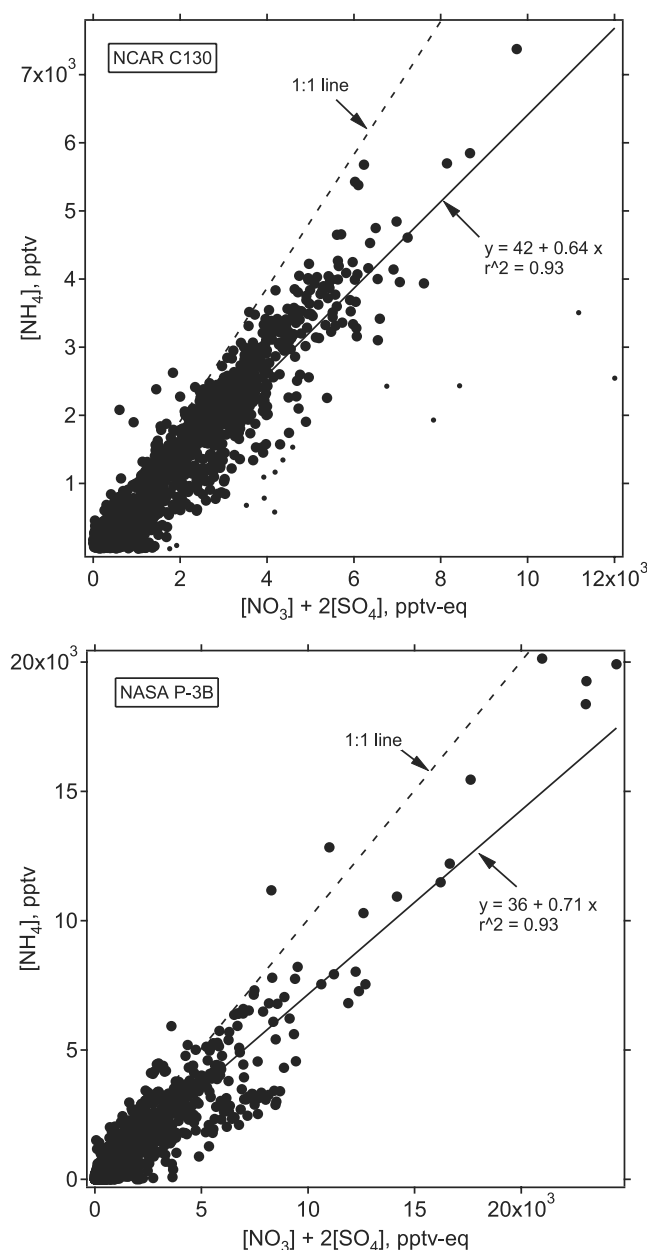


**Figure 10.** Correlation between  $\text{NH}_4^+$  and the sum of  $\text{NO}_3^-$  and  $\text{SO}_4^{2-}$ . The solid lines represent the least squares best fits. The data points showing a significant departure from the main group were not used (small solid circles, top panel).

magnitude of percent deviation from a complete charge balance below the total concentration of 3 ppbv. Above that, the P-3B data showed a smaller positive deviation (10–15%) and a negative deviation comparable to that of the C130 data.

[26] Since the limit of detection of the PILS-IC were  $10 \text{ ng m}^{-3}$  and  $50 \text{ ng m}^{-3}$  for the anions and cations, respectively [Orsini *et al.*, 2003], we estimate a measurement uncertainty in the total anion to be  $\sim 10 \text{ pptv}$  and total cation to be  $\sim 110 \text{ pptv}$ . The total uncertainty in the ion imbalance calculation is  $\sim 110 \text{ pptv}$ , being dominated by the cation's uncertainty. It is clear that this small measurement

uncertainty contributed negligibly to the observed scatter in Figure 16, accounting for only 10% at a total concentration as low as 1 ppbv. One notes, however, that the higher LOD for cations may be responsible for a larger negative deviation in charge balance at the lowest aerosol mass loading because values below LOD were assigned as zero.

[27] It is noted that one should not consider only those samples exhibiting charge imbalance to have unmeasured ions. Since neither organic ions nor the strong acid, hydronium ion, were measured, it is unlikely that we can rule out the presence of these components for samples

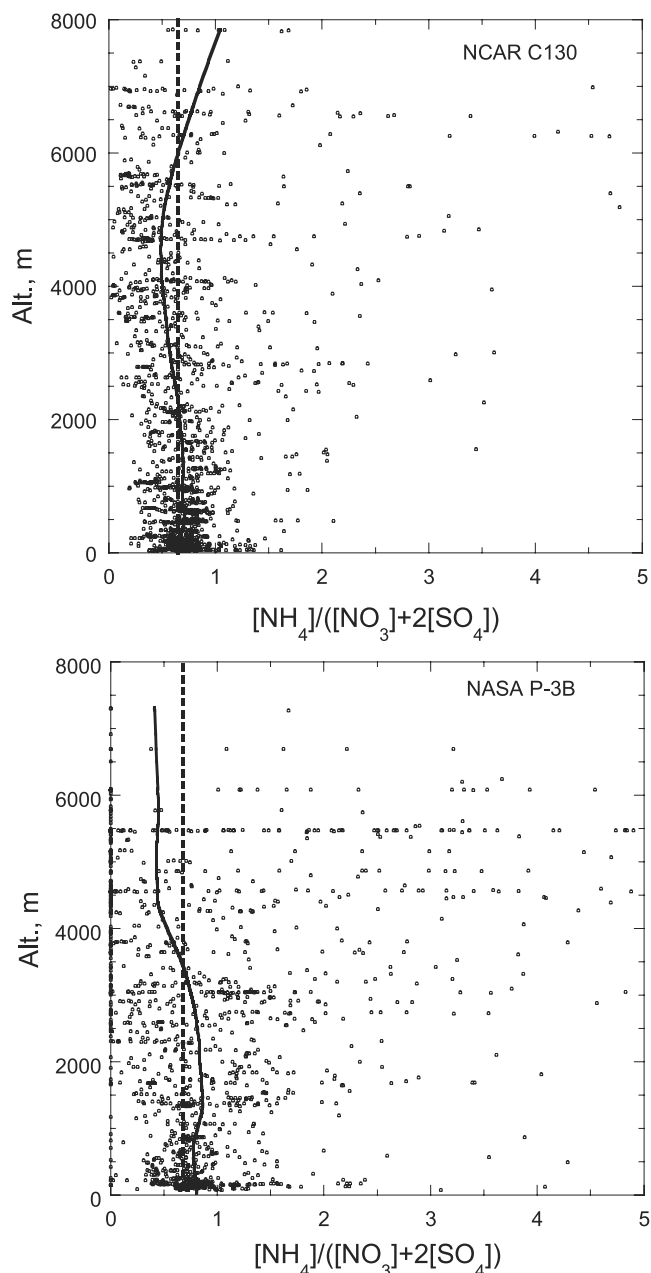


**Figure 11.** Altitude dependence of the ratio of  $\text{NH}_4^+$  to the sum of  $\text{NO}_3^-$  and  $\text{SO}_4^{2-}$ ; values greater than 5 not shown. The solid curve represents the Lowess fits, which approximates the median values. The dotted lines are the slopes of the best fits in Figure 10.

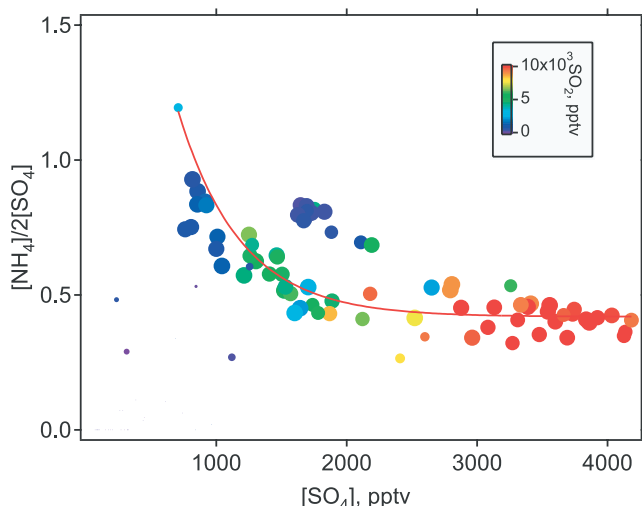


**Figure 12.** Ratio of  $[\text{NH}_4^+]$  to  $2[\text{SO}_4^{2-}]$  as a function of aerosol sulfate concentration observed during a volcano plume study (NASA P-3B flight 17, 27 March 2001). Data are color-coded to  $\text{SO}_2$  concentration and size-coded to altitude (large circles for 2 km and below). The exponential fit of the data is limited to those associated with the Miyakejima volcanic plume using  $[\text{SO}_2] > 2$  ppbv as a criterion. Note that the maximum  $\text{SO}_2$  was 17 ppbv, extending beyond the color bar scale.

that did show a reasonable charge balance. Two corollaries that follow are (1) no a priori expectation of a normally distributed charge balance centered at zero based on the 8 measured ions, and (2) the missing charges can only be

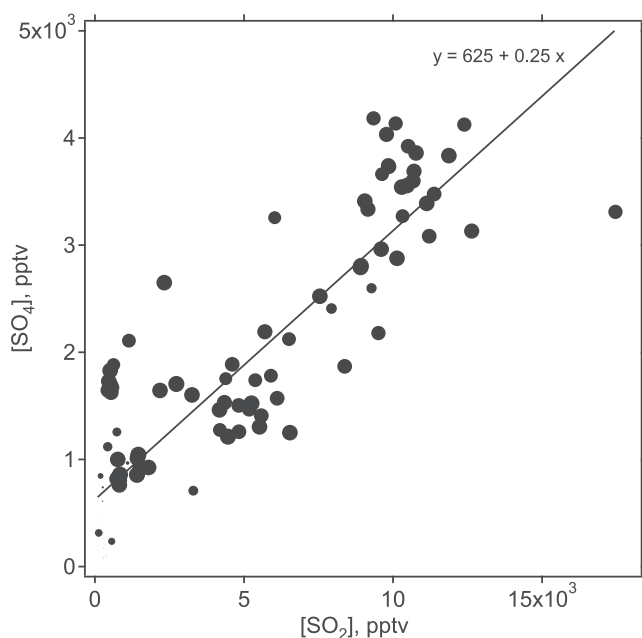


**Figure 13.** Relationship between aerosol  $\text{SO}_4^{2-}$  and  $\text{SO}_2$  in the Miyakejima volcano plume. The solid line represents the best fit of the data for  $\text{SO}_2 > 2$  ppbv ( $r^2 = 0.80$ ). Data points collected at 2 km and below are represented by the large circles.

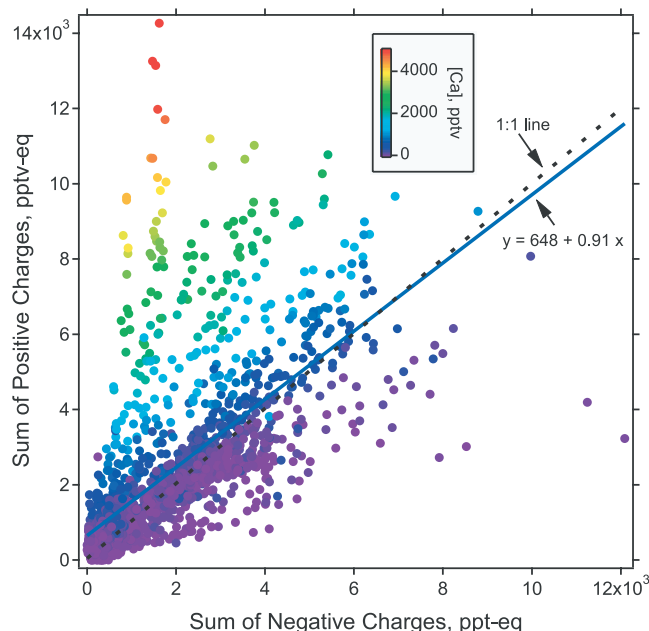


**Figure 14.** Plot of the total positive charges against the total negative charges of the aerosol ionic components measured on the NCAR C130 aircraft. Data points are color-coded to  $\text{Ca}^{2+}$  concentration; the solid line is the least squares fit of the data.

used to arrive at lower limit estimates for the concentrations of unmeasured ionic species.

### 3.3. Altitude Dependence of Charge Imbalance

[28] We plot the charge imbalance as a function of altitude in Figure 17 to inspect whether a systematic dependence exists. The Lowess fits of the C130 data show that the surrogate median value is very near zero at the lowest altitude, and increases with increasing altitude reaching +60% at the maximum altitude of 8 km. With  $\text{Ca}^{2+}$  removed, we note that the median remains at  $\sim$ zero from the lowest altitude to 5 km and then increases to +30% at the highest altitude. The data points with total ion concentration less than 500 pptv which are expected to show the largest percent measurement uncertainties ( $\geq 20\%$ , Figure 17) did not show a significantly different pattern in either magnitude or sign of the departure from the remaining data, indicating that measurement uncertainties contributed insignificantly to the observed charge imbalance. The P-3B data showed an increase in positive deviation with increasing altitude, similar to the C130 data. However, the lower concentration data points (total ion  $< 500$  pptv) appeared to exhibit a wider spread in the imbalance, suggesting that measurement uncertainties were partly responsible for the observed charge imbalance.

### 3.4. Relationships of Aerosol Ionic Components With Other Measurements

[29] Fine aerosol particles are known to have an important source in combustion processes which produce precursors such as  $\text{SO}_2$ , hydrocarbons, and  $\text{NO}_x$  in addition to primary particulate matter such as soot containing particles. Since CO is a major byproduct of combustion, a correlation between CO and fine aerosol mass loading (and some

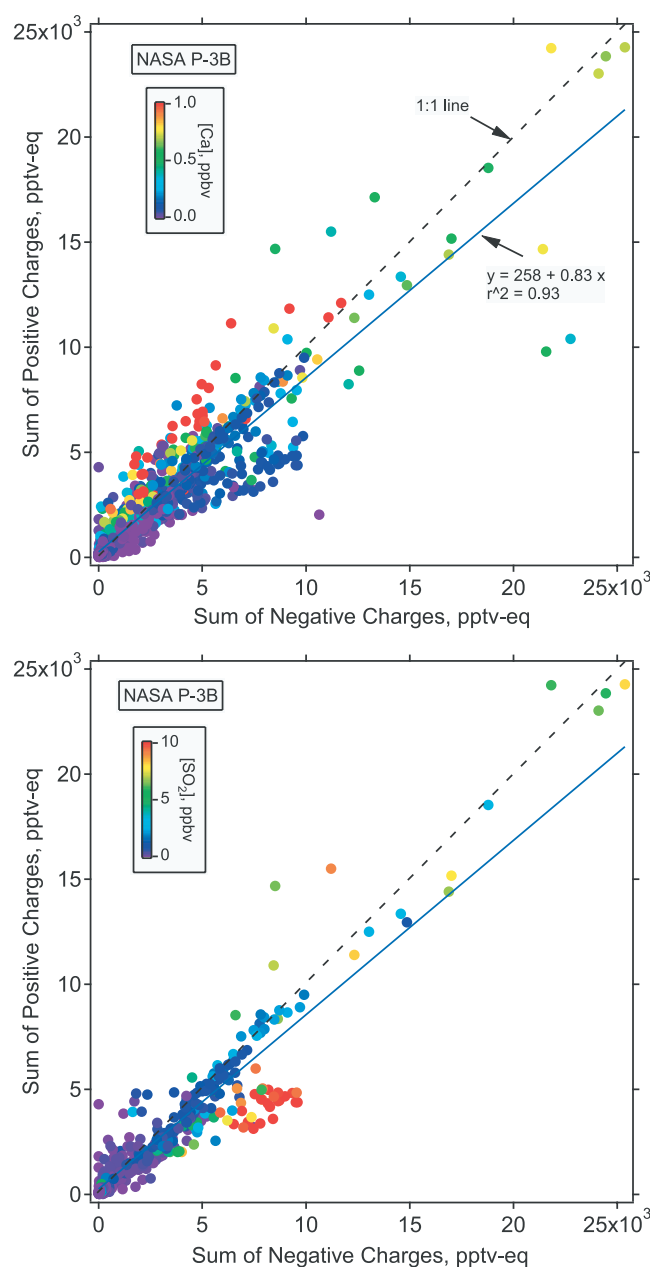


**Figure 15.** Plot of the total positive charges against the total negative charges of aerosol ionic components measured on the NASA P-3B. (top) Color-coded to  $\text{Ca}^{2+}$  concentration. (bottom) Color-coded to  $\text{SO}_2$  concentration. The two solid lines are the same and represent the best fit of the data points in the top graph.

aerosol chemical components) is expected. In Figure 18 we plot the sum of the concentrations of  $\text{NH}_4^+$ ,  $\text{SO}_4^{2-}$ ,  $\text{NO}_3^-$ , and  $\text{K}^+$  against  $[\text{CO}]$ .  $\text{Na}^+$ ,  $\text{Cl}^-$ ,  $\text{Ca}^{2+}$ , and  $\text{Mg}^{2+}$  were not included because they are considered noncombustion related. Although the majority of the C130 data points conform to a fairly strong correlation (Figure 18), there is a separate group of samples that showed much smaller ratios, i.e.,  $[\text{CO}]$  ranging between 250 and 1000 ppbv with corresponding  $[\text{total ion}]$  between 0 and 1 ppbv. Since these data points also correspond to similarly low ratios of other species to CO, e.g., toluene and ethane, we surmise that

these data points were collected in air masses that had been substantially processed, e.g., by photo chemical reactions, leaving, however, the long-lived CO relatively unchanged.

[30] To investigate this possibility, we establish a time scale that can approximate the photochemical age of an air mass using the measured hydrocarbon concentrations. Ratios of co-emitted hydrocarbons, e.g., benzene and toluene from automobile exhausts, have been applied to determining the plume age [Gelencser *et al.*, 1997]. While this approach has the advantage of being insensitive to dilution, good knowledge of the ratios of the hydrocarbons at the source is required. Further, a realistic average OH concentration is also needed. Since fairly large uncertainties exist in both quantities, the photochemical age estimated here is at best qualitative. However, somewhat favorable for the

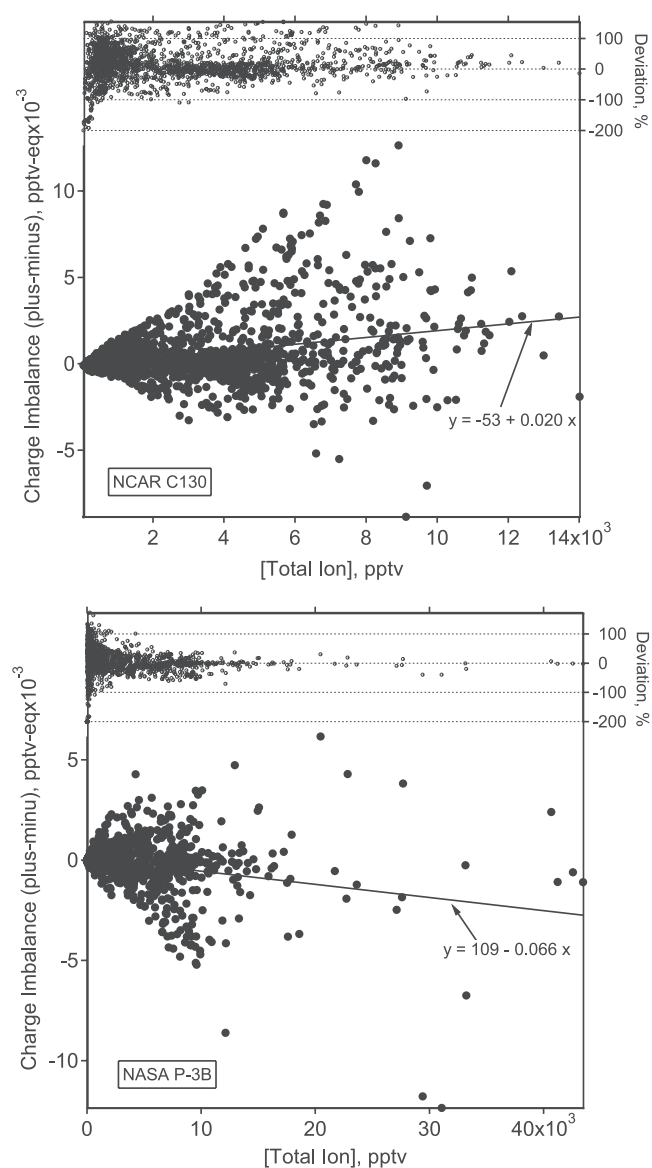


**Figure 16.** Charge imbalance of the measured aerosol ionic components as a function of total ion concentration. The solid line represents the best fit of the data, and the top panel in each graph shows the imbalance normalized to total ion concentration.



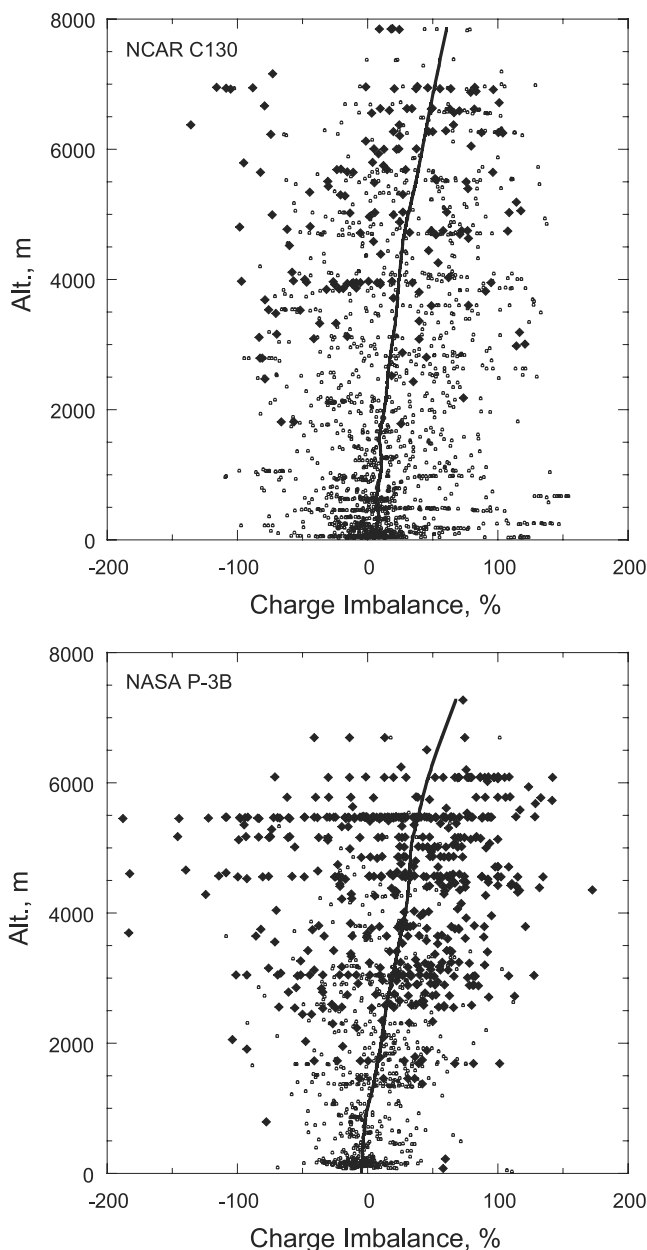


**Figure 17.** Charge imbalance as a function of altitude. Points with a total ion concentration less than 500 pptv are shown as solid diamonds. The solid lines represent Lowess fits to the data.

ACE-Asia and TRACE-P environment is that there are fewer nearby sources over the ocean that can confound this ratio.

[31] From the selected hydrocarbon species available we used ethyne and toluene for this calculation because both are known to have a strong source in vehicular emissions. Using a source ethyne/toluene ratio of 0.65 [Fraser *et al.*, 1998] and a 24-hr average [OH] of  $5.5 \times 10^6 \text{ cm}^{-3}$ , we derived a photochemical age ranging from 8 hr to 51 hr (C130). This time scale agreed with that established using propane and toluene to within 10 hrs. Although the C130 data in Figure 18 showing a small ion mass to CO ratio were somewhat aged, 30 to 51 hr, there are significantly more

data points in this age group belonging to the higher slope group of Figure 18. Consequently, it is clear that photochemical reactions ( $\sim 2$  days) were not the primary process by which aerosols were removed from the atmosphere. Cloud processing which preferentially removes soluble species is likely to be responsible for the low [ions] to [CO] ratios in these samples. Since cloud processing is often accompanied by rise of air masses to higher altitudes,

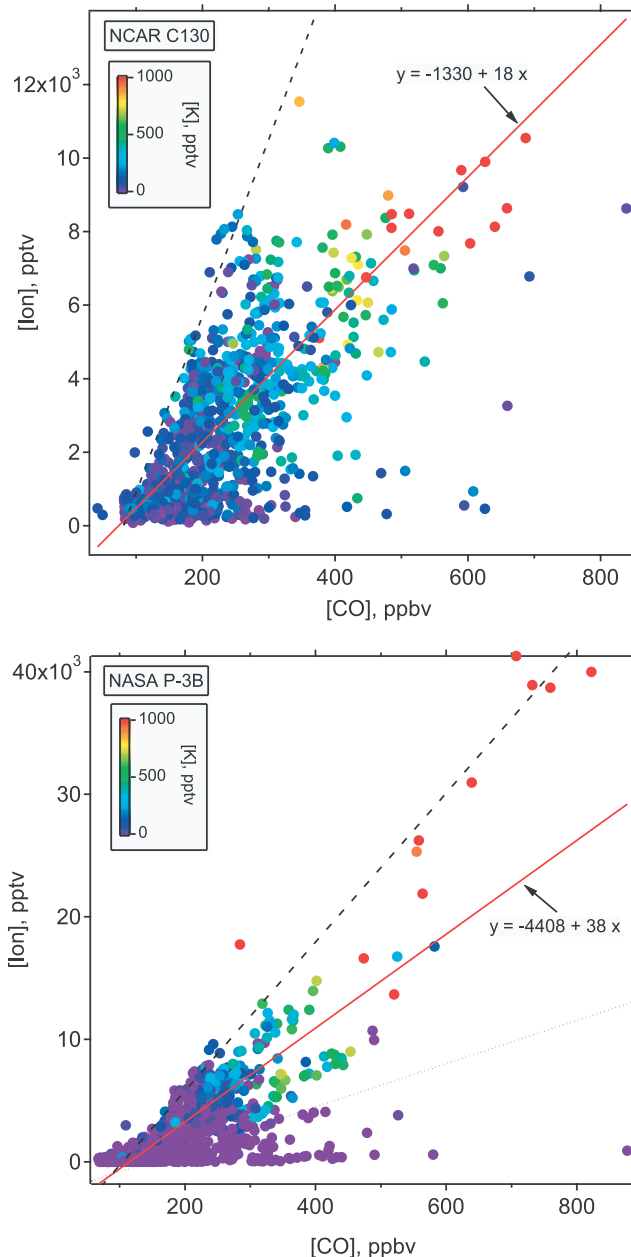


**Figure 18.** Correlation between the sum of combustion related aerosol ionic components ( $\text{NO}_3^-$ ,  $\text{SO}_4^{2-}$ ,  $\text{NH}_4^+$ , and  $\text{K}^+$ ) and CO. The solid lines represent the best fits of the data without the group of points showing high [CO] (>250 ppbv) and low [ion] (<1 pptv),  $r^2$  being 0.67 and 0.76, respectively. The dashed lines are the eyeballed top edge of the data envelope. The dotted line in the bottom panel is the best fit line of the NCAR C130 data.

samples collected at higher altitudes may have increased chance of going through such a process. In this regard, we note that 31 of the 34 samples in this group were collected at altitude greater than 2 km.

[32] We note that the inclusion of the noncombustion related ions did not affect the correlation, with the  $r^2$  remaining at 0.82. This is not unexpected concerning  $\text{Na}^+$  and  $\text{Cl}^-$  as their concentrations were low. However, this also indicates that  $\text{Ca}^{2+}$  which was present at much higher concentrations had been relatively well mixed with combustion-derived plumes. Furthermore, it is worth noting that in Figure 18 samples containing elevated  $\text{K}^+$  are associated with high  $[\text{CO}]$ . Since  $\text{K}^+$  is believed to be a tracer for biomass (and biofuel) burning, the inefficient combustion process which is known to generate a significant amount of CO is corroborated by this observation.

[33] A brief diversion follows. It should be cautioned that the qualitative photochemical age analysis carried out here is based on the assumption that vehicular-derived urban pollution in large Chinese cities (e.g., Shanghai) is similar in character to that of the U.S. However, the validity of this assumption may be partly supported by two considerations. First, China has a policy in place keeping vehicles older than 10 years off the road and as a result the fleet is dominated by modern vehicles, most of them produced in China by major international nameplates. Second, despite the fact that the air sampled on the P-3B were impacted by various regions, including Hong Kong, Japan, Korea and China, tight correlation between several key hydrocarbon species (e.g., toluene, benzene, i-pentane, n-butane) were observed on the P-3B similar to those observed in North America [e.g., Parrish *et al.*, 1998],

[34] A similar analysis is made for the P-3B data in Figure 18. Although  $\text{K}^+$  is again found to be associated with high  $[\text{CO}]$ , the data did not form clearly distinguishable groups like the C130 data. We nonetheless fitted the data without the group which showed  $[\text{ion}]$  less than 1 ppbv and  $[\text{CO}]$  greater than 250 ppbv. The slope of the best fit line is nearly twice as that for the C130 data, resulting possibly from less aged high concentrations of pollution encountered by the P-3B. It may be pointed out that the photochemical age of the most polluted urban plume encountered (the first plume in Figure 6) was estimated to be  $\sim 20$  hr using the benzene/toluene pair. These low ion-high CO samples were found to have elevated  $\text{CH}_3\text{Cl}$  (600–1000 pptv), but contained essentially zero  $\text{K}^+$ , consistent with cloud processing which had preferentially removed the soluble species. The altitude at which these points were sampled ranged between 0.6 and 6 km with 49 out of 72 at above 2 km. The eyeballed maximum slopes using the top of the data envelopes (dashed lines, Figure 18) are fairly similar between the C130 and the P-3B, providing a qualitative estimate for the ion (including precursors) to CO emission ratio of 5% at the sources.

### 3.5. Relationship Between $\text{Ca}^{2+}$ and $\text{NO}_3^-$

[35]  $\text{Ca}^{2+}$  (and other mineral cations) contained in dust aerosols serves as an important neutralizing and quenching reagent for acids produced in the gas phase (e.g., nitric and sulfuric acids). Although it has been suggested that mineral particles can also mediate chemical transformation [Dentner *et al.*, 1996] by way of surface reactions oxidizing  $\text{NO}_2$  to

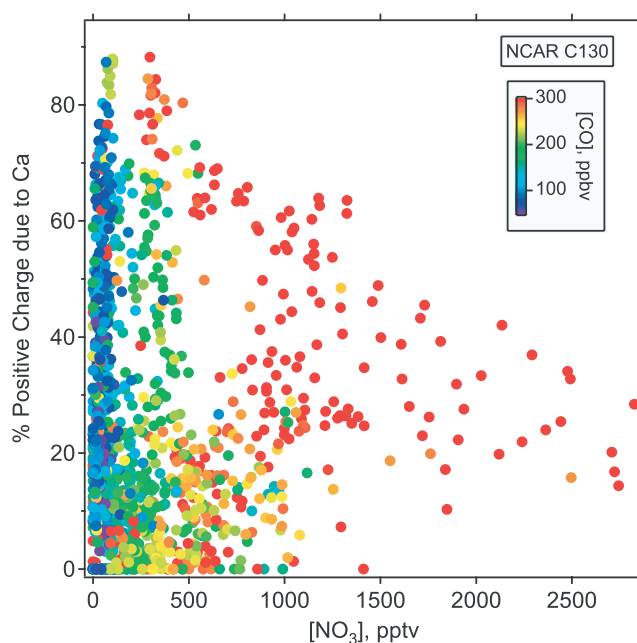


**Figure 19.** The contribution of  $\text{Ca}^{2+}$  to positive charges as a function of aerosol nitrate concentration.

$\text{NO}_3^-$ , field observations needed to support this mechanism have not been unequivocally established. A major difficulty in verifying this pathway lies in the fact that gas phase formation of  $\text{HNO}_3$  from  $\text{NO}_2$  oxidation by OH followed by adsorption onto mineral particles is typically fast, characteristic  $\text{NO}_2$  life time being  $< 24$  hr. The data collected on the C130 and P-3B again showed that samples of high aerosol  $[\text{NO}_3^-]$  are associated with high  $[\text{CO}]$  where active photochemical production of  $\text{HNO}_3$  is expected. In Figure 19 we plot the percent positive charge due to  $\text{Ca}^{2+}$  as a function of aerosol  $[\text{NO}_3^-]$ . While it is clear that  $\text{Ca}^{2+}$  played an important role as a neutralizing reagent, accounting for up to  $\sim 50\%$  of the positive charges at  $[\text{NO}_3^-] \sim 1.5$  ppbv, elevated  $[\text{NO}_3^-]$ , i.e., greater than 200 pptv, were nearly exclusively associated with  $[\text{CO}] \geq 200$  ppbv. Photochemical formation of  $\text{HNO}_3$  in polluted air followed by its adsorption onto  $\text{Ca}^{2+}$  containing aerosol particles is a plausible mechanism for the observation of Figure 19. Only the C130 data were shown because of the larger  $\text{Ca}^{2+}$  concentration observed on this platform.

## 4. Conclusions

[36] Fine aerosol ionic components,  $\text{NH}_4^+$ ,  $\text{SO}_4^{2-}$ ,  $\text{NO}_3^-$ ,  $\text{K}^+$ ,  $\text{Ca}^{2+}$ ,  $\text{Mg}^{2+}$ ,  $\text{Na}^+$ , and  $\text{Cl}^-$ , were determined at a 4-min time resolution using the PILS-IC technique on board the NCAR C130 and NASA P-3B aircraft during the ACE-Asia and TRACE-P experiment, respectively. The maximum total ion concentration observed on the P-3B was  $84 \mu\text{g m}^{-3}$ , significantly higher than that on C130,  $27 \mu\text{g m}^{-3}$ , because of encountering of a highly polluted air mass over the Yellow Sea. The timing and location, however, allowed the C130 to sample air masses that were heavily impacted by dust particles indicated by the elevated  $\text{Ca}^{2+}$  concentrations (maximum = 6 ppbv). Low levels of  $\text{Mg}^{2+}$  were also derived from dust at a  $\text{Mg}/\text{Ca}$  ratio of  $\sim 0.16$ . Higher levels of

Mg were found to have a sea-salt origin showing a Mg/Na ratio of  $\sim 0.1$ .  $\text{Cl}^-$  and  $\text{Na}^+$  were in general correlated, the slope being close to their seawater ratio. However, additional sources of  $\text{Cl}^-$  in urban emissions and dust plumes were also indicated.  $\text{SO}_4^{2-}$ ,  $\text{NO}_3^-$ , and  $\text{K}^+$  all showed strong correlations with CO, consistent with their combustion origins.  $\text{NH}_3$ , which appeared to also be co-emitted from the combustion processes and urban areas, was comparable in supply to  $\text{H}_2\text{SO}_4$  and its precursor  $\text{SO}_2$ , responsible for neutralizing  $\sim 70\%$  of the total aerosol acidity. Charge balance of the 8 measured ions showed that although the positive and negative charges are tightly correlated, slope  $\geq 0.8$ , the magnitude of the imbalance (positive charge minus charge, in pptv-eq) was  $\geq 20\%$  of the total ion concentration (in pptv). It is expected that these missing charges are associated with organic acids and bases, and to a lesser extent, the hydronium ion. The unmeasured chemical components were likely to also be present even in cases where an apparent charge balance was observed. The charge imbalance did not show an altitude dependence and was not significantly influenced by measurement uncertainties. The presence of  $\text{NO}_3^-$  in  $\text{Ca}^{2+}$  containing aerosol particles was noted and may result from adsorption of photochemically produced  $\text{HNO}_3$  onto the  $\text{Ca}^{2+}$  containing particles.

[37] **Acknowledgments.** This research was supported by NSF and NOAA Office of Global Change Program for the ACE-Asia Project and by NASA GTE for the TRACE-P Project. The participation of YNL in the ACE-Asia and TRACE-P was supported by NOAA through an interagency agreement and by NASA through a subcontract with Georgia Institute of Technology, respectively. We thank T. Anderson of U. of Washington for helpful comments and suggestions.

## References

- Andreae, M. O., and P. Merlet, Emission of trace gases and aerosols from biomass burning, *Global Biogeochem. Cycles*, **15**, 955–966, 2001.
- Blake, N. J., D. R. Blake, T.-Y. Chen, J. E. Collins Jr., G. W. Sachse, B. E. Anderson, and F. S. Rowland, Distribution and seasonality of selected hydrocarbons and halocarbons over the western Pacific basin during PEM-West A and PEM-West B, *J. Geophys. Res.*, **102**, 28,315–28,331, 1997.
- Dentner, F. J., G. R. Carmichael, Y. Zhang, J. Lelieveld, and P. Crutzen, Role of mineral aerosol as a reactive surface in the global troposphere, *J. Geophys. Res.*, **101**, 22,869–22,889, 1996.
- Fraser, M. P., G. R. Cass, and B. R. T. Simoneit, Gas-phase and particle-phase organic compounds emitted from motor vehicle traffic in a Los Angeles roadway tunnel, *Environ. Sci. Technol.*, **32**, 2051–2060, 1998.
- Gelencser, A., K. Siszler, and J. Jlavay, Toluene-benzene concentration ratio as a tool for characterizing the distance from vehicular emission sources, *Environ. Sci. Technol.*, **31**, 2869–2872, 1997.
- Kawamura, K., and F. Sakaguchi, Molecular distributions of water soluble dicarboxylic acids in marine aerosols over the Pacific Ocean including tropics, *J. Geophys. Res.*, **104**, 3501–3509, 1999.
- Lee, Y.-N., Z. Song, Y. Liu, P. Daum, R. Weber, D. Orsini, N. Laulainen, J. Hubbe, and V. Morris, Aerosol chemical characterization on board the DOE G1 aircraft using a particle-into-liquid-sampler during the TexAQS 2000 experiment, paper presented at 82nd Annual AMS Meeting, Am. Meteorol. Soc., Orlando, Fla., 13–17 Jan., 2002.
- Ma, Y., et al., Characteristics and influence of biosmoke on the fine particle ionic composition measured in Asian outflow during TRACE-P, *J. Geophys. Res.*, **108**(D21), 8816, doi:10.1029/2002JD003128, in press, 2003.
- Marple, V. A., and K. Willeke, Impactor design, *Atmos. Environ.*, **10**, 891–896, 1976.
- National Research Council (NRC), Research priorities for airborne particulate matter: I. Immediate priorities and a long-range research portfolio, Comm. on Res. Priorities for Airborne Particulate Matter, Washington, D. C., 1998.
- Orsini, D. A., Y. Ma, A. Sullivan, B. Sierau, K. Baumann, and R. J. Weber, Refinements to the particle-into-liquid sampler (PILS) for ground and airborne measurements of water soluble aerosol composition, *Atmos. Environ.*, **37**, 1243–1259, 2003.
- Parrish, D., et al., Internal consistency tests for evaluation of measurements of anthropogenic hydrocarbons in the troposphere, *J. Geophys. Res.*, **103**, 22,339–22,359, 1998.
- Perrino, C., M. Catrambone, A. Di Menno Di Bucchianico, and I. Allegrini, Gaseous ammonia in the urban area of Rome, Italy and its relationship with traffic emission, *Atmos. Environ.*, **36**, 5385–5394, 2002.
- Sachse, G. W., J. E. Collins Jr., G. F. Hill, L. O. Wade, L. G. Burney, and J. A. Ritter, Airborne tunable diode laser system for high precision concentration and flux measurements of carbon monoxide and methane, *Proc. SPIE Int. Opt. Eng.*, **1433**, 145–156, 1991.
- Seinfeld, J. H., and S. N. Pandis, *Atmospheric Chemistry and Physics: From Air Pollution to Climate Change*, John Wiley, Hoboken, N. J., 1997.
- Sioutas, C., P. Y. Wang, S. T. Ferguson, P. Koutrakis, and J. D. Mulik, Laboratory and field evaluation of an improved glass honeycomb denuder/filter pack sampler, *Atmos. Environ.*, **30**, 885–895, 1996.
- Thornton, D. C., A. R. Bandy, F. H. Tu, B. W. Blomquist, G. M. Mitchell, W. Nadler, and D. H. Lenschow, Fast airborne sulfur dioxide measurement by Atmospheric Pressure Ionization Mass Spectrometry (APIMS), *J. Geophys. Res.*, **107**(D22), 4632, doi:10.1029/2002JD002289, 2002.
- Wang, Z., H. Akimoto, and I. Uno, Neutralization of soil aerosol and its impact on the distribution of acid rain over east Asia: Observations and model results, *J. Geophys. Res.*, **107**(D19), 4389, doi:10.1029/2001JD001040, 2002.
- Weber, R. J., D. A. Orsini, Y. Duan, Y.-N. Lee, P. J. Klotz, and F. Brechtel, A particle-into-liquid collector for rapid measurement of aerosol bulk chemical composition, *Aerosol Sci. Technol.*, **35**, 718–727, 2001.
- Ye, B., X. Ji, H. Yang, X. Yao, C. K. Chan, S. H. Cadle, T. Chan, and P. A. Mulawa, Concentration and chemical composition of PM<sub>2.5</sub> in Shanghai for a 1-year period, *Atmos. Environ.*, **37**, 499–510, 2003.
- A. Bandy, D. Thornton, and F.-H. Tu, Department of Chemistry, Drexel University, Philadelphia, PA 19104, USA.
- D. Blake and S. Meinardi, Department of Chemistry, University of California, Irvine, CA 92697, USA.
- T.-Y. Chen, Environmental Change Research Project, Academia Sinica, Taipei 11529, Taiwan.
- C. Harward and G. Sachse, NASA Langley Research Center, Hampton, VA 23681, USA.
- Y.-N. Lee, Atmospheric Sciences Division, Brookhaven National Laboratory, Upton, NY 11973, USA. (ynlee@bnl.gov)
- Y. Ma, K. Maxwell-Meier, D. Orsini, and R. Weber, School of Earth and Atmospheric Sciences, Georgia Institute of Technology, Atlanta, GA 30332, USA.